Electronics and Electrical Engineering

AIMS Electronics and Electrical Engineering, 9(3): 314–338.
DOI: 10.3934/electreng.2025015
Received: 24 March 2025
Revised: 13 May 2025
Accepted: 26 May 2025
Published: 06 June 2025

https://www.aimspress.com/journal/ElectrEng

Research article

A comparative study on time-delay estimation for time-delay nonlinear system control

Syeda Nadiah Fatima Nahri*, Shengzhi Du, Barend J. van Wyk and Oluwaseun Kayode Ajayi

Department of Electrical Engineering, Faculty of Engineering and the Built Environment, Tshwane University of Technology, Pretoria 0001, South Africa

*** Correspondence:** Email: nadiyah9490@gmail.com.

Abstract: Time delay and disturbances are commonly encountered in real-world application systems, and their existence significantly hampers the operation of various controllers available in the discipline of control systems theory. Time-delay estimation and disturbance compensation are closely related to obtaining the desired system stability and efficient controller operation. This paper discusses state-of-the-art methods for time-delay estimation (TDE)-based methods related to active disturbance rejection control (ADRC) methods and proportional-integral-derivative (PID) controllers found in the latest literature on control systems theory. The methodology includes simulation designs incorporating the integration of predictive extended state observer-based ADRC (PESO-ADRC) and conventional PID controllers with the TDE mechanism, followed by their respective control on systems with time delay and disturbances. A comparative analysis performed on the TDE compensation methods highlights that TDE enhances the robustness to time delay, various uncertainties, and nonlinear dynamics existing in the controlled system. The time-varying delay, nonlinear backlash-like hysteresis, and an added system external disturbance were considered in the simulation. The performance was measured based on specific transient response characteristics such as the rise time, settling time, overshoot criteria, and performance index measures such as the integral of time-weighted absolute error (ITAE) and the percentage of improvement by the decrease in overshoot given by P_i (%). Further, a sensitivity analysis of TDE parameters to the controllers' operation was also performed. Experimental results indicate stability and a strong capacity to regulate the transient and steady-state responses under the impact of various uncertainties. Therefore, the comparative analysis conducted between TDE-ADRC and TDE-PID control methods signifies the importance of TDE with disturbance compensation in time-delayed systems, commonly found in real-world industrial applications.

Keywords: active disturbance rejection control (ADRC); proportional-integral-derivative control (PID); time-delay estimation (TDE); disturbance compensation; nonlinearity; time-delay control

1. Introduction

In the domain of automation and teleoperation systems, time delays and uncertainties are significantly associated with inefficient operation of the overall control system [1–3]. This is mainly due to factors like time delay, hysteresis, parameter perturbation, external disturbances, and noise, which are inevitable in real-world system applications. Moreover, besides external output disturbances acting on a system, uncertainties like nonlinear backlash-like hysteresis, nonlinear components' interaction with their surroundings, and time delay persist in communication channels for a controlled object/plant, causing nonlinearity in a control system. Hence, this requires designing and improving robust disturbance rejection controllers with a time-delay estimation (TDE) mechanism to obtain stable and steady-state transient system responses.

Several model-based and model-free control approaches have been developed over time. The former is affected by the system's parameter uncertainty and unmodelled dynamics. In contrast, the latter considers a variety of system uncertainties, including internal and external disturbances, nonlinear hysteresis, sensor noise, and varying time delay [4–6].

In the literature, one of the most widely employed model-free controllers is an active disturbance rejection control (ADRC), whose model is updated continually to perform disturbance compensation in time-delay control [7,8]. Han first developed the ADRC in the mid-1990s [9], followed by its application by Gao [7]. The characteristic feature of the ADRC controller is its ability to measure internal and external disturbances actively, generally coined as "total disturbance", and then compensate for these total disturbance effects in real-time via the feedback loop. This is accomplished with an extended state observer (ESO), an integral feature of the ADRC controller [7].

Further, the time delay aspect is the most crucial aspect that greatly impairs the performance of the controlled system. Impairments include response overshooting with oscillations, reduced damping ratio, and moving the closed-loop system response to instability. Thus, controller design becomes more challenging due to the time delay and the different forms of disturbances to the system, which need to be controlled. Therefore, to mitigate the effects of different types of uncertainties acting on a concerned system, the ESO component has been amended over time to accommodate the ADRC operation in industrial applications; for example, in robotic systems [10], power plants [11], teleoperation systems [12], and piezoelectric-related medical fields [13]. Such modifications in the control law helped attain a decent trade-off between disturbance rejection and controller operation in a concerned time-delayed system.

Furthermore, another widely used and established industrial controller, called the proportional-integral-derivative (PID) controller, has evolved over time. The PID controller depicts decent accomplishment in overcoming various nonlinearities, such as the chattering effect, delay, and external disturbances present in robotic industries [14]. However, despite consistent efforts to conquer the time-delay problem, the adverse effects of delay are still difficult to overcome. Thus, time-delay estimation followed by compensation is still a work in progress for various disturbance rejection control methods [15,16]. Moreover, recent research has shown that the performance of an ADRC controller concerning estimation and attenuation of nonlinear backlash-like hysteresis under

time delay and uncertainties is greatly improved in conjunction with TDE mechanisms [8,17]. Other controller methods commonly used in integration with the TDE mechanism for attenuation of system nonlinearities include, for example, the PID controller [18], adaptive sliding mode controller (SMC) [19], and fuzzy logic approach-based [20] control methods. These methods are reviewed in the following subsection.

1.1. Literature survey

As an estimation technique, TDE mainly estimates the unknown dynamics of the controlled system by using the system's delayed dynamics. Usually, the TDE method is used in conjunction with other control strategies to attain the necessary uncertainty compensation and enhanced system transient steady-state performance. Some examples from the literature include TDE with PID control, ADRC-based control, SMC, and fuzzy-based control.

One of the TDE-PID approaches in [18] provides a unified TDE-based PID-nonsingular terminal SMC that takes advantage of both PID characteristics and the terminal SMC (TSMC) to manage cable-driven manipulators with matching disturbance. However, it was recommended that the mismatched disturbance be studied. Further, to estimate and counteract nonlinearity, such as friction and external system disturbance in a robotic manipulator, a modified TDE method was constructed by combining a fractional-order TSMC with PID [21]. It was recommended that future work address varying system time delays.

Furthermore, to supervise robotic manipulators impacted by hysteresis and external system disturbances, a robust controller was designed by combining the TDE with a nonsingular PID and a fast TSMC [22]. This approach used the fuzzy system to regulate PID gains. Future research will enhance the system's performance when dead-zone nonlinearity and applied measurement noise are present. Moreover, to counteract the adverse effects of complex lumped uncertainties and backlash hysteresis on system performance, an adaptive robust TSMC approach employing the TDE method has been developed for robotic manipulators [23], followed by multivariable fast TSMC for cable-driven manipulators [24]. Future research will examine chattering effects, dead zones, saturation, and noise reduction.

In another study [25], an ADRC predicted and attenuated the nonlinearities in an all-clamped plate system by applying the TDE definition to the ESO in the frequency domain. However, future research will analyze the external disturbances impacting the controlled object. Therefore, in most TDE-based methods, it has been observed that the stability and performance of the controller design are greatly impaired under the influence of external disturbances and varying system time-delay circumstances. Hence, in this paper, a comparative analysis is performed in terms of estimation and compensation of uncertainties based on experimental responses and performance measurement criteria on recently proposed control methods, namely the predictive TDE-based ADRC method [8] and a TDE-based PID control method [17], which will be employed to control a given system termed the controlled object.

2. Methodologies used in the controller designs

This section describes the preliminary mathematical concepts used to design the complete TDE-based predictive ESO-based ADRC and the TDE-based PID controllers. These are experimentally analyzed under different case studies in Section 3.

2.1. System or controlled object description

For simplicity and reliability, most controllers focus on lower-order, simpler models for analysis, as higher-order systems are frequently examined using lower-order ones (usually the second-order approximation) in control theory. The second-order system used in this analysis is represented by the state-space equation given by Equation (1).

$$\begin{cases} \dot{x}(t) = Ax(t) + Bu(t) + f(x(t), t) \\ y(t) = C^T x(t - \tau) \\ x(0) = [0 \quad 0]^T \end{cases} \tag{1}$$

where the system state vector is given by $x(t) = [x_1(t), x_2(t)]^T$, and the system output is $y(t)$. Matrix A is the state transition, B is the input, and C is the output matrix of the concerned system/plant. The dimensions of these matrices are given by $A \epsilon \mathbb{R}^{(n\times n)}$, $B \epsilon \mathbb{R}^{(n\times 1)}$, and $C \epsilon \mathbb{R}^{(1\times n)}$. $n = 2$ for the system shown in Equation (1). The system time delay is indicated by τ, and the control signal to the system is given by $u(t)$. $f(x(t), t)$ is the total disturbance acting on the system, which includes input and output disturbances, nonlinear backlash-like hysteresis, and unknown system dynamics.

2.2. Time-delay estimation mechanism

TDE is a method for estimating system disturbance that uses time-delayed input from the preceding sampling event. The sampling period, represented by t_s in Equations (2) and (3), is a small delay that the TDE technique introduces when constructing a controller. Consequently, the TDE reduces the total effect of cumulative disturbances. Equation (3) presents the TDE law, as shown in Figure 1.

$$\hat{\zeta}(t) = \zeta(t - t_s) \tag{2}$$

$$\zeta(t - t_s) = u_a(t - t_s) - \eta \ddot{y}(t - t_s) \tag{3}$$

where $(t - t_s)$ represents the time-delayed value, and $\hat{\zeta}(t)$ indicates the estimate of all uncertainties. $\ddot{y}(t - t_s)$ represents the dynamics of the delayed system output. The parameter η, which is a positive nominal value, is adjusted to obtain the best feasible controller performance. Furthermore, when the sample period t_s decreases, the estimate $\hat{\zeta}(t)$ gets stronger as the TDE can operate effectively, according to Equation (3). Moreover, for robotic manipulators, η is given by a diagonal matrix [26].

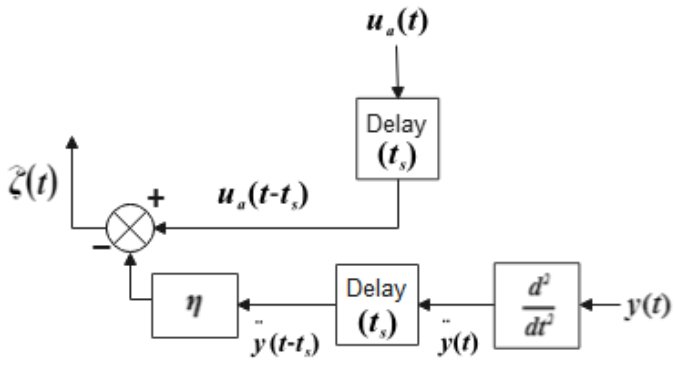

Figure 1. Time-delay estimation approach.

Hence, the proposed hypothesis in this study utilizes the TDE approach with an additional control method to achieve the required performance and steady-state transient system response. Thus, in this comparative study, it will be demonstrated that the robustness of the TDE mechanism is advantageous when combined with the predictive ESO-based ADRC and PID controllers individually by combating various system nonlinear uncertainties impacting the time-delay system and, therefore, will improve the controlled system's quality.

2.3. Hysteresis model: Duhem backlash-like hysteresis model

The hysteresis effect is widely acknowledged to affect the precision of both closed-loop and open-loop control systems and lead to persistent oscillations. This highlights how a change in the direction of an input signal can alter the response of an output signal, thus introducing nonlinear behavior in control systems theory [27,28]. Therefore, in control systems, hysteresis can result in oscillation, instability, and incorrect positioning. Hence, it may prove challenging to develop controllers that can precisely follow the intended trajectory due to nonlinear behavior. The Duhem model given in [8,26] contributes to dynamic hysteresis in this study. Equations (4) and (5) are the foundation for the mathematical description of the Duhem backlash-like hysteresis framework. Constants α, β, and γ correspond to hysteresis constants and are greater than 0; also, $\alpha > \beta$.

$$\frac{dw(v)}{dx} = \gamma \left|\frac{dv}{dt}\right| \left(\alpha v - w(v)\right) + \beta \frac{dv}{dt} \tag{4}$$

$$w(v) = \alpha v(t) + [w_0 - \alpha v_0] e^{-\gamma (v - v_0)\text{sign}\,(\dot{v})} + e^{-\gamma v \text{sign}\,(\dot{v})} \int_{v_0}^{v} (\beta - \alpha)\, e^{-\gamma \varepsilon \,\text{sign}\,(\dot{v})} d\varepsilon \tag{5}$$

wherein the initial conditions of the input v and output w are v_0 and w_0, respectively. For an input signal $v(t) = \rho \sin(2.5\, t)$, the response of the Duhem hysteresis curve in Figure 2 is generated for ρ = 2 using the model parameter values γ = 1, α = 1.16, and β = 0.35. Also, the initial values w_0 and v_0 are set to zero.

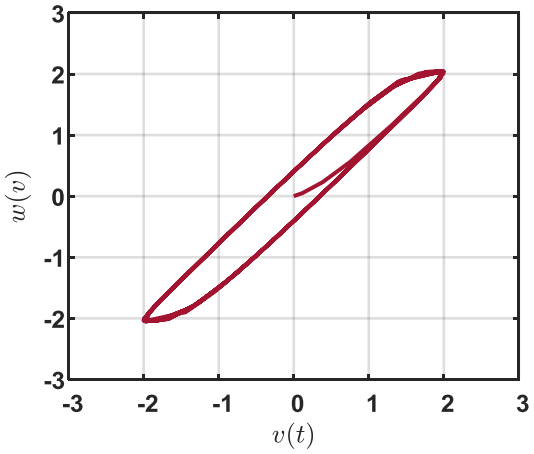

Figure 2. Backlash-like hysteresis response (Duhem).

2.4. ADRC with a delayed input system

An ADRC consists of three primary subsystems: a tracking differentiator (TD), a nonlinear state

error feedback (NLSEF) controller, and the extended state observer (ESO) [7]. The block diagram of a basic ADRC structure with delayed input is given in Figure 3 [29]. The ESO is a fundamental element of the ADRC that actively estimates and compensates for the overall disturbance $f(t)$ imposed on the controlled object given by Equation (1).

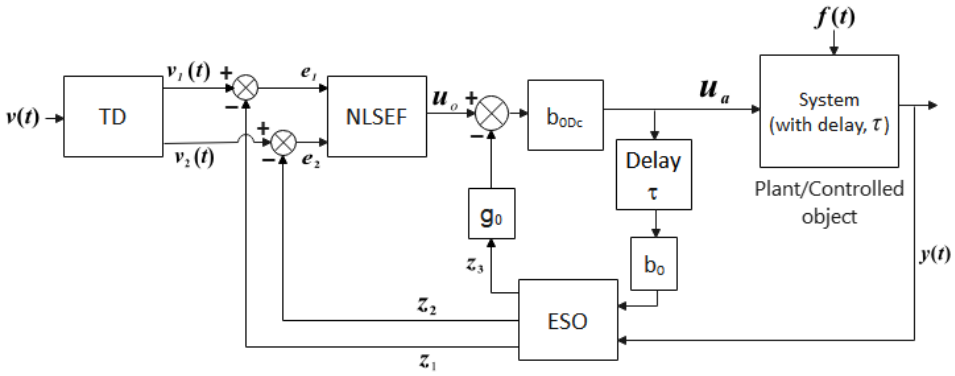

Figure 3. Block diagram of ADRC with delayed input for a controlled object (system).

In Figure 3, the TD produces a softer signal with an estimated derivative signal. By extracting the difference signals e_1 and e_2 from the TD-generated signals $v_1(t)$ and $v_2(t)$ and the ESO-generated estimated system states z_1 and z_2, the NLSEF produces the control law denoted by u_0.

The TD and NLSEF equations for Figure 3 are given by Equations (6), (7), and (8).

$$\begin{cases} \dot{v}_1 = v_1 + hv_1 \\ \dot{v}_2 = v_2 + h\text{fhan}(v_1 - r, v_2, r_0, h) \end{cases} \tag{6}$$

where $v_1(t)$ and $v_2(t)$ are softened and differentiated signals obtained by supplying TD with the reference signal $v(t)$. Thus, TD improves the reference input reactivity while producing the intended transient profile. By setting r_0 to r and applying the nonlinear function $\text{fhan}(v_1 - r, v_2, r_0, h)$, which is defined by a series of relations in Equation (8), the fastest convergence from v_1 to v with the least amount of overshoot is achieved [7]. The TD parameters denote the simulation step and the transition process speed r_0 and h, respectively. The nonlinear function fhan has equations in stages that are provided in [7,30], with the NLSEF's signal output u_o.

$$\begin{cases} e_1 = v_1 - z_1 \\ e_2 = v_2 - z_2 \\ u_o = -\text{fhan}(e_1, c \cdot e_2, r, h_1) \end{cases} \tag{7}$$

Equation (7) displays the NLSEF parameters, given by control gain r, simulation step c, and damping coefficient h_1. The optimal controller response is achieved by adjusting these NLSEF controller parameters.

$$\begin{cases} d = r_0 h^2 \\ a_0 = h v_2 \\ y = v_1 - v + a_0 \\ a_1 = \sqrt{d(d + 8|y|)} \\ a_2 = a_0 + \left[\frac{\text{sign}\,(y)(a_1 - d)}{2}\right] \\ s_y = \frac{[\text{sign}\,(y+d) - \text{sign}\,(y-d)]}{2} \\ a = (a_0 + y - a_2)s_y + a_2 \\ s_a = \frac{[\text{sign}\,(a+d) - \text{sign}\,(a-d)]}{2} \\ \text{fhan} = -r_0\left(\frac{a}{d} - \text{sign}(a)\right)s_a - r_0 \text{sign}(a) \end{cases} \tag{8}$$

For Figure 3, the ESO equations and the control law are stated in Equations (9) and (10), respectively [30].

$$\begin{cases} e = z_1 - y \\ \dot{z}_1 = z_2 - \beta_{01} e \\ \dot{z}_2 = z_3 - \beta_{02}\,\text{fe} + b_0 u_a(t-\tau) \\ \dot{z}_3 = -\beta_{03}\,\text{fe}_1 \end{cases} \tag{9}$$

$$u_a = (u_0 - z_3 g_0) b_{0\text{Dc}} \tag{10}$$

where the ESO gains are given by β_{01}, β_{02}, and β_{03}. Parameters b_0 and g_0 are additional gain factors, whereas $b_{0\text{Dc}}$ represents the disturbance compensation factor. The nonlinear feedback functions fe and fe_1 are defined as $\text{fe} = \text{fal}(e, 0.5, h_{ESO})$ and $\text{fe}_1 = \text{fal}(e, 0.25, h_{ESO})$, respectively. For $\alpha < 1$, the error (e) will decrease to zero more quickly. The simulation step size of ESO is denoted by h_{ESO}. The complete estimated disturbance signal is denoted by z_3. The controlled object (system) has u_a as its control signal and y as its output signal. Equation (11) provides the nonlinear function fal value [30].

$$\text{fal}(e, \alpha, \varepsilon) = \begin{cases} \frac{e}{d^{1-\alpha}}, |e| \le \varepsilon \\ |e|^{\propto}\text{sign}(e), |e| > \varepsilon \end{cases} \tag{11}$$

2.4.1. Block diagram of TDE integration with predictive ESO-based ADRC controller (TDE-PESO-ADRC)

As seen in Figure 4, the predictive ESO-based ADRC (PESO-ADRC) mechanism is derived by combining the ADRC with the input that is delayed (shown in Figure 3) and the extended state predictor observer (ESPO) [31], to predict the unknown dynamics of the concerned system that were generated as a disturbance amid the delay. The estimated disturbance $\hat{\delta}(t)$ is then removed from $u_a(t)$ to provide sufficient compensation for the total disturbance.

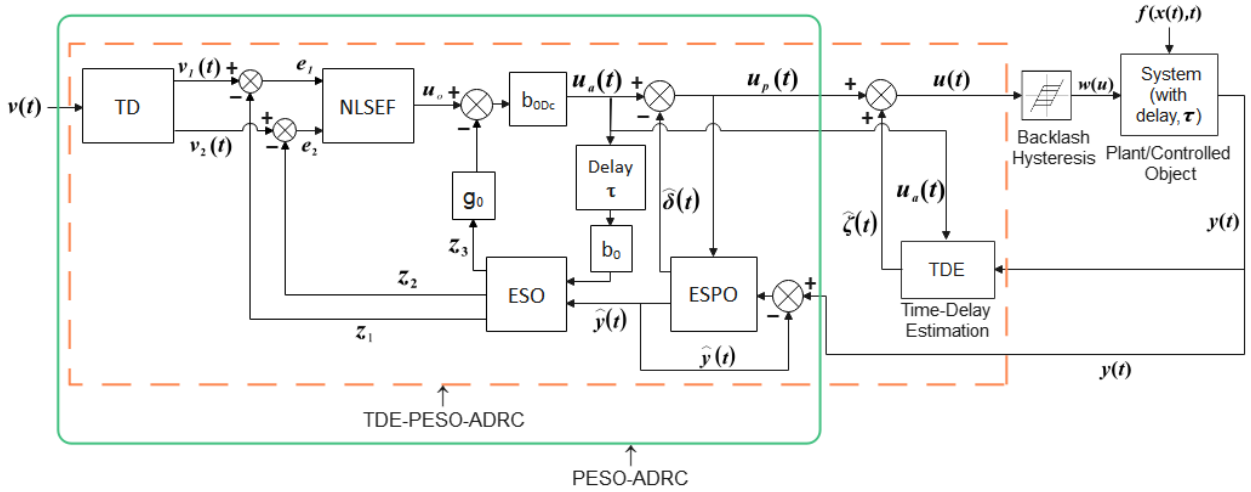

Figure 4. Block diagram of TDE-predictive ESO-based ADRC (redrawn from [8]).

The ESPO is expressed in the literature by a series of mathematical equations [30,31]. An essential component of the ESPO is observer bandwidth (ω_e), which is adjusted to produce the required system response. The Hurwitz stability criterion regulates the selection of ω_e; thus, the complete details of the ESPO used in this study are outlined in [30,31]. Moreover, as seen in Figure 4, the estimation error fed to the ESPO is defined as the difference between the system output $y(t)$ and the estimated system output $\hat{y}(t)$. Hence, the TDE-based predictive ESO-based ADRC is a cascaded arrangement of the PESO-ADRC with the TDE mechanism. The complete structure is denoted as the TDE-PESO-ADRC controller method.

Equation (12) represents the overall disturbance ($\delta(x(t),t)$) affecting the controlled object,

$$\delta(x(t),t) = f(x(t),t) + w(v_m) \tag{12}$$

where $f(x(t),t)$ is inclusive of the external output disturbance applied and parameter perturbation in the system under time-delay control. $w(v_m)$ is the nonlinear Duhem backlash-like hysteresis given by Equations (4) and (5).

The TDE-PESO-ADRC controller's control law, $u(t)$, is given by Equation (13),

$$\begin{cases} u(t) = u_p(t) + \hat{\zeta}(t) \\ \quad\quad = (u_a(t) - \hat{\delta}\,(t)) + \left(u_a(t-t_s) - \eta\ddot{y}(t-t_s)\right) \end{cases} \tag{13}$$

where $\hat{\zeta}(t)$ is the TDE mechanism given by Equations (2) and (3). Also, $u_p(t)$, the control law for the PESO-ADRC, is given in Equation (14) [8].

$$\begin{cases} u_p(t) = u_a(t) - \hat{\delta}\,(t) \\ \quad\quad = (u_0(t) - z_3 g_0) b_{0\mathrm{Dc}} - \hat{\delta}\,(t) \\ \quad\quad = (-\mathrm{fhan}(e_1, c\cdot e_2, r, h_1) - z_3 g_0) b_{0\mathrm{Dc}} - \hat{\delta}\,(t) \end{cases} \tag{14}$$

2.4.2. Block diagram of the TDE-based PID control method (TDE-PID)

The PID controller is one of the most widely used control processes in the field of industrial applications [32]. When nonlinearity or disturbance is added to a PID-controlled system, it drives the system to instability or inadequate performance. Thus, improving the conventional PID controller's operation is important, as it requires modifying its control law to achieve the desired tracking performance of the object to be controlled via optimal control operation.

In this study, the TDE-PID controller developed in [17] is analyzed. The integrated TDE-PID controller's structure is pictorially presented in Figure 5.

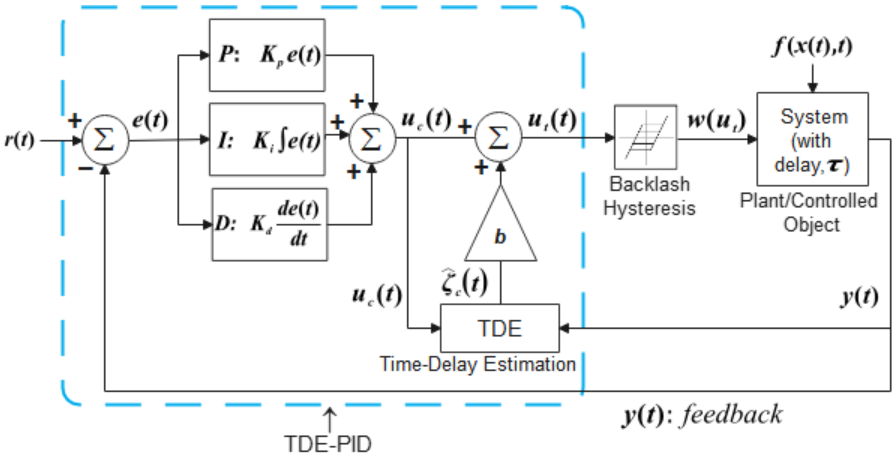

Figure 5. Block diagram of TDE-based PID control (redrawn from [17]).

The time-delay system to be controlled is given by Equation (15).

$$\begin{cases} \dot{x}(t) = Ax(t) + Bu_c(t) + f(x(t), t) \\ y(t) = C^T x(t - \tau) \end{cases} \tag{15}$$

where $u_c(t)$ is the control law of the conventional PID controller. Other variables in Equation (15) are defined in Equation (1).

The control law $u_t(t)$ of the cascaded TDE-PID controller structure is given in Equation (16).

$$\begin{cases} u_t(t) = u_c(t) + b\,\hat{\zeta}_c(t) \\ \qquad = u_c(t) + b\big(u_c(t - t_s) - \eta\ddot{y}(t - t_s)\big) \\ \qquad = (K_p e(t) + K_i \int e(t)dt + K_d \frac{de(t)}{dt}) + \\ \qquad\qquad b\big(u_c(t - t_s) - \eta\ddot{y}(t - t_s)\big) \end{cases} \tag{16}$$

where $r(t)$ is the input reference signal fed to the TDE-PID-controlled system. The standard PID control law $u_c(t)$ is the cumulative sum of the proportional (P), integral (I) and derivative (D) segments, along with their respective gains K_p, K_i, and K_d, respectively. $e(t)$ is the variation between the output signal $y(t)$ and the input signal $r(t)$. The gain factor b is utilized to tune the contribution from TDE to the control variable $u_t(t)$. The TDE equation for the TDE-PID control method in Figure 5 is given by Equation (17).

$$\hat{\zeta}_c(t) = \big(u_c(t - t_s) - \eta\ddot{y}(t - t_s)\big) \tag{17}$$

For a given sampling period t_s and constant η in Equation (17), the delayed input and output dynamics are indicated by $u_c(t-t_s)$ and $\ddot{y}(t-t_s)$, respectively.

3. Experimental results and discussions

The recent works in [8] and [17] presented control of a time-delay system by a cascaded TDE with a predictive ESO-based ADRC and the PID control method, respectively. Thus, this section performs a comparative analysis of the two TDE-based methods to discuss their performance measures and transient responses under different control scenarios. As specified in section 2.1, the controlled object considered in the experimental analysis is a second-order system with a time delay. Such a system is chosen as a benchmark system under testing for various industrial plants. The system concerned is represented in its transfer function form by Equation (18).

$$G(s) = \frac{2}{s^2+3s+2}e^{-\tau s} = \frac{1}{(s+1)(0.5s+1)}e^{-\tau s} \tag{18}$$

When Equation (18) is represented in its state-space form, seen in Equation (1), the state-space matrix values obtained are $A = \begin{bmatrix} -3 & 1 \\ 2 & 0 \end{bmatrix}$, $B = \begin{bmatrix} 0 \\ 2 \end{bmatrix}$, $C = [1 \quad 0]$; and system delay τ = 0.1 s.

The ADRC controller parameters of the PESO-ADRC method were obtained by optimizing the delayed input ADRC structure shown in Figure 2 using the genetic algorithm (GA) tool of MATLAB software version R2020a in the *Optimization tools* window [30]. On optimization, the controller parameter values attained are c = 0.7645, h_1= 1.0831, r = 56.0350, g_o = 0.3097, b_0 = 3.1303, and $b_{0\mathrm{Dc}}$ = 1.0314. Further, the fixed parameter values of the TD component are r_0 = 10 and h = 0.03; also, the remaining parameters of the ESO components are given by $[\beta_{01}, \beta_{02}, \beta_{03}, h_{ESO}]$ = [100, 300, 1000, 0.01] [33]. Furthermore, the observer bandwidth ω_e of the ESPO is tuned to obtain the desired system behavior, and its selection is based on the Hurwitz stability definition defined in [30,31]. Moreover, for the PID controller, the parameter values K_p, K_i, and K_d were manually tuned to 1, 0.8, and 0.1, respectively. The gain factor b was set to 0.2 [17]. Also, the input signal given to both controlled structures is a unit step.

In the experiments that follow, the robustness of the TDE-based controller designs is analyzed based on certain transient system response characteristics like rise time [RT (s)], response time [t_r (s)], settling time [ST (s)], and overshoot [OV (%)] under the impact of different uncertainties. Further, the controller performance is evaluated using the system performance index measure termed integral of time-weighted absolute error (ITAE) and is also evaluated based on the improvement of performance percentage, P_i (%), of all the specified transient characteristics, given in Equation (19):

$$P_i\,(\%) = \left(1 - \frac{P_1}{P_0}\right) \times 100 \tag{19}$$

where P_1 and P_0 represent the response characteristic parameters for TDE-based and non-TDE-based control strategies, respectively.

3.1. Experiment 1: Impact of TDE on control mechanisms in the absence of uncertainties

In this analysis, PID and PESO-ADRC control strategies are assessed in the presence and absence of the TDE method for the case of no uncertainties (disturbances and nonlinearity) acting on the time-delayed system in Equation (18). For TDE-based PID control, the TDE parameters are η =

0.01 and t_s = 0.001 s; for TDE-based PESO-ADRC control, the parameters are η = 0.2 and t_s = 0.002 s. The observer bandwidth is ω_e= 3 and τ = 0.1 s. Figure 6 illustrates the system responses obtained, and Table 1 tabulates the control performance criteria for both control strategies when tested with and without the TDE mechanism.

It was observed that with the TDE present, the controlled system rose faster for both control scenarios (TDE-PID and TDE-PESO-ADRC), i.e., for the PID controller RT = 1.5263 s with TDE, and RT = 1.8958 s without the TDE mechanism. A similar improvement in rise time of 23.81% is also obtained for the TDE-PESO-ADRC method. Further, the settling time, ITAE value, and overshoot are decreased by 62.07%, 52.26%, and 55.25%, thus showing a greater performance improvement for PESO-ADRC with TDE control. However, a significant improvement in performance measures was not obtained in the case of the TDE-PID control method in comparison to its non-TDE structure, as seen in Table 1. Hence, under this scenario, the integration of TDE with the ADRC strategy provided a better response than its respective non-TDE version and TDE-PID control approach.

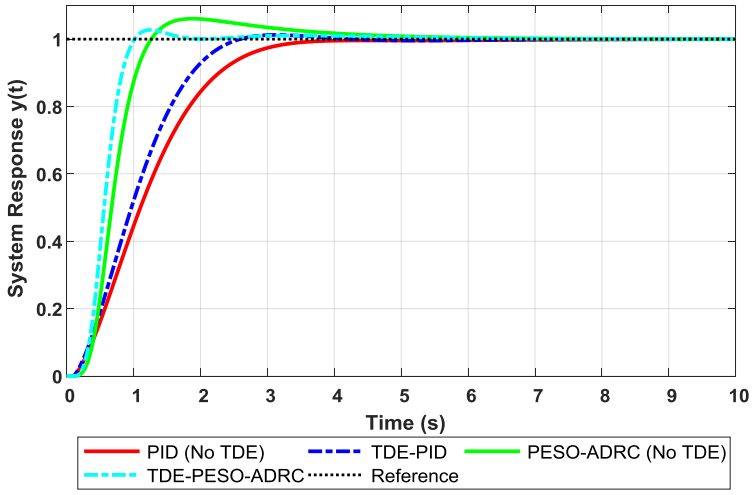

Figure 6. System response impact of TDE on PID and PESO-ADRC methods.

Table 1. Control performance criteria for PID and PESO-ADRC controllers with and without TDE mechanism.

Control method	Performance criteria	TDE excluded	TDE included	P_i (%)
PID	RT (s)	1.8958	1.5263	19.4905
	ST (s)	3.1252	2.3384	25.1760
	OV (%)	0.0000	1.2581	-
	ITAE	1.1220	0.8018	28.5383
PESO-ADRC	RT (s)	0.6481	0.4938	23.8080
	ST (s)	3.7868	1.4363	62.0709
	OV (%)	6.0380	2.7019	55.2517
	ITAE	0.6016	0.2872	52.2606

3.2. Experiment 2: Impact of TDE on control mechanisms in the presence of nonlinear hysteresis

In this study, the effectiveness of the control strategy of the TDE approach cascaded with the PID and PESO-ADRC controllers is investigated on a time-delay system, as given in Equation (18),

under the influence of nonlinear backlash-like hysteresis represented by Equations (4) and (5). The term $w(v_m)$ in Equation (12) depicts the dynamic hysteresis output. For the PID controller, the variables used for hysteresis are γ = 2, α = 1.16, and β = 0.35, whereas for the predictive ADRC controller, the variables are γ = 0.1, α = 1.16, and β = 0.35. Moreover, the TDE parameters for both PID and predictive ADRC methods are η = 0.01, t_s = 0.001 s, τ = 0.1 s, and η = 0.001, t_s = 0.001 s, and τ = 0.1 s, respectively. The ESPO observer bandwidth is ω_e = 4.

Figure 7 and Table 2 demonstrate the effectiveness of the TDE mechanism in counteracting the nonlinear nature of the hysteresis effect on the PESO-ADRC method. Meanwhile, the TDE mechanism improved performance for the PID controller regarding quicker settling time, smaller steady-state error, and smaller ITAE. However, as shown in Table 2, there is a minimal decrease in system overshoot in the TDE-PID control strategy and a longer rising time.

Further, the ITAE index measure with the TDE present is 2.1260 and 1.0130 for both PID and PESO-ADRC controllers, respectively, which shows an improvement of 64.74% and 81.23% as compared to without the TDE approach present. Furthermore, by integrating the TDE with the predictive ADRC method, the system response in Figure 7 shows robustness and thus less oscillatory behavior, reduced overshoot, and quick system recovery to uncertainties, contrary to the TDE-PID system response and performance.

Table 2. Control performance criteria for PID and PESO-ADRC controllers under hysteresis.

Control method	Performance criteria	TDE excluded	TDE included	P_i (%)
PID	RT (s)	1.1511	1.3818	-20.0417
	ST (s)	15.5398	6.0472	61.0857
	OV (%)	11.9685	11.8873	0.6784
	ITAE	6.0290	2.1260	64.7371
PESO-ADRC	RT (s)	0.6705	0.4032	39.8658
	ST (s)	10.8993	4.8639	55.3742
	OV (%)	43.6208	20.8107	52.2918
	ITAE	5.3960	1.0130	81.2268

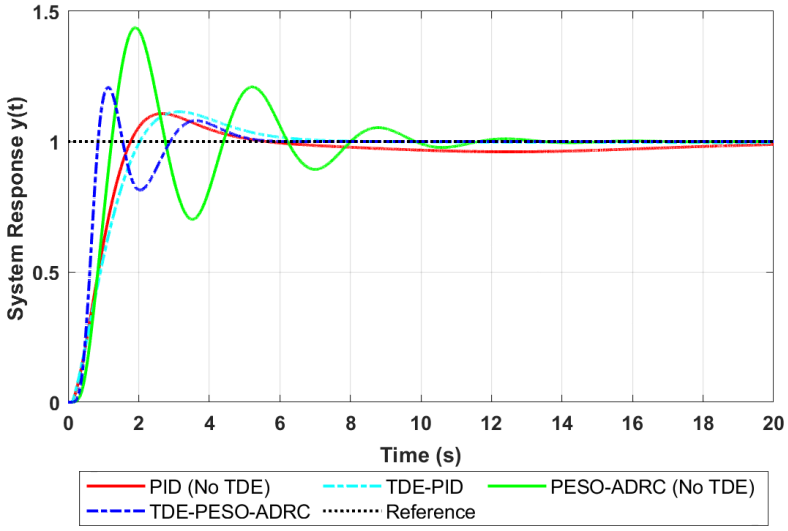

Figure 7. System response impact of TDE on PID and PESO-ADRC methods under nonlinear hysteresis.

3.3. Experiment 3: Impact of TDE on control mechanisms in the presence of nonlinear hysteresis and perturbed system parameter

This section provides an experimental analysis for the case of nonlinear hysteresis and parameter perturbation present as uncertainties in the time-delayed system in Equation (18) under control. In this simulation, 25% of parameter perturbation is inserted at 20 s under hysteresis for both the system time constants and the system time delay. Hence, the perturbed system transfer function for Equation (18) is given by Equation (20).

$$\tilde{G}(s) = \frac{1.28}{s^2+2.4s+1.28} e^{-0.125s} \quad ; \qquad \begin{cases} \dot{\tilde{x}} = \tilde{A}\tilde{x} + \tilde{B}u \\ \tilde{y} = \tilde{C}\tilde{x} \end{cases} \tag{20}$$

where $\tilde{A} = \begin{bmatrix} -2.40 & 1 \\ -1.28 & 0 \end{bmatrix}$, $\tilde{B} = \begin{bmatrix} 0 \\ 1.28 \end{bmatrix}$ and $\tilde{C} = [1 \quad 0]$.

Perturbed system delay, $\tilde{\tau}$ = 0.125 s. For PID with TDE control, the TDE parameters considered are η = 0.01 and t_s = 0.001 s. Further, for PESO-based ADRC with TDE control, the TDE parameters considered are η = 0.001, t_s = 0.001 s, τ = 0.125 s, and ω_e = 4. Furthermore, for hysteresis, the variables in PID control are γ = 2, α = 1.16, and β = 0.35; and for PESO-ADRC, the variables are γ = 0.1, α = 1.16, and β = 0.35.

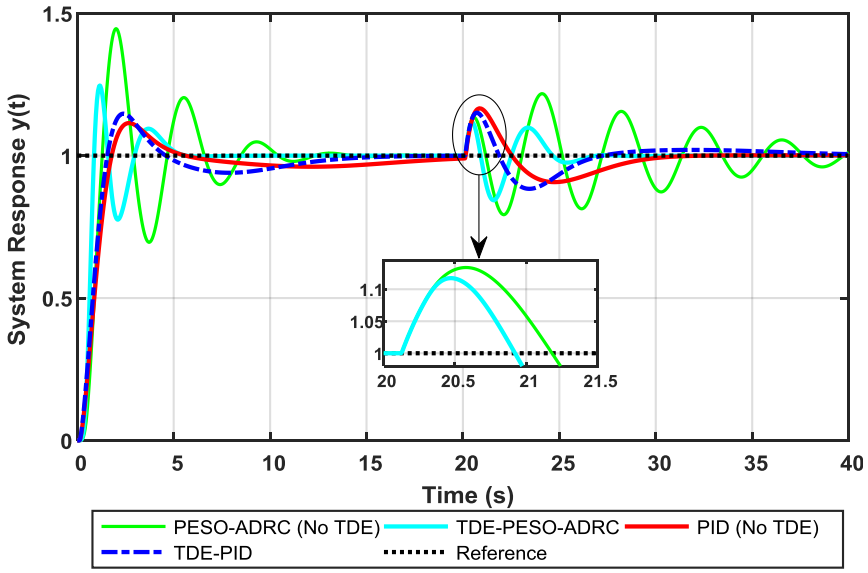

Figure 8. System response impact of TDE on PID and PESO-ADRC methods under nonlinear hysteresis and perturbed system parameters.

The perturbed system's performance measures are displayed in Figure 8 and listed in Table 3. Table 3 and Figure 8 demonstrate that the systems responded more quickly and had a shorter rise when TDE was present. The RT was 1.0316 s with TDE vs 1.1677 s without TDE for the PID control scheme, and 0.4007 s with TDE compared to 0.7052 s without TDE for the PESO-ADRC approach. For the TDE-PESO-ADRC method, the initial system response's overshoot was greatly reduced by 45%; however, for the case of PID with TDE, the decrease in initial overshoot was not observed. However, from Table 3, under the effect of parameter perturbation at 20 s, the TDE system reached a

faster settling time for the cases of both TDE with PID and PESO-ADRC control approaches. Hence, the percentage improvement P_i obtained in ST, ITAE, and OV was significant for the predictive ADRC-TDE control (34.79%, 80.44%, and 42.64%, respectively), contrasted to the TDE-PID control method, thus showing greater robustness to the concerned system's perturbed parameters and nonlinear hysteresis acting under time-delay control.

Table 3. Control performance criteria for PID and PESO-ADRC controllers under hysteresis and parameter perturbation.

Control method	Performance criteria	TDE excluded	TDE included	P_i (%)
PID	RT (s)	1.1677	1.0316	11.6554
	ST (s)	28.9399	26.4470	8.6141
	OV (%)	16.4865	14.4684	12.1317
	ITAE	21.7600	21.7700	≈ 0
PESO-ADRC	RT (s)	0.7052	0.4007	43.1792
	ST (s)	39.5763	25.8071	34.7915
	OV (%)	42.9332	24.6245	42.6446
	ITAE	49.8300	9.7460	80.4415

3.4. Experiment 4: Impact of TDE on control mechanisms in the presence of nonlinear hysteresis, perturbed system parameters, and added external disturbance

This experiment extends the one from the preceding subsection, which included hysteresis and a 25% incrementation in system parameters at 20 s. Thus, the cumulative applied uncertainty given by Equation (12) includes the nonlinear hysteresis, parameter perturbation, and input disturbance in the form of external disturbance added to the perturbed system in Equation (20). Two different forms of external disturbances are assessed in this section. Case 1 is a step input disturbance of magnitude 0.6 applied at 20 s, $f_1(x(t), t)$ stated in Equation (21), and the other case is with periodic forms of uncertainties $f_2(x(t), t)$ given by Equation (22).

$$f_1(x(t), t) = 0.6\,\mathrm{step}(t - \theta) \tag{21}$$

$$f_2(x(t), t) = 0.4\sin(x_1) - 0.1u + 0.2\,(\sin\frac{\pi}{8t}) \tag{22}$$

For hysteresis, under all cases, the variables used are γ = 2, α = 1.16, and β = 0.35. Under case 1, for TDE-PID, η = 0.01 and t_s = 0.001 s, whereas for TDE-PESO-ADRC, η = 0.001 and t_s = 0.001 s. Other parameters for the ADRC and PID controllers are equal to those specified in the preceding section. Figures 9 and 10 illustrate the impact on system responses for both TDE-PID and TDE-PESO-ADRC controllers under the nonlinear effects of hysteresis, perturbed system parameters, and an added input external disturbance to the perturbed time-delay system. Table 4 lists the corresponding performance metrics for Figures 9 and 10.

As indicated in Table 4, Figures 9 and 10 demonstrate that both the controlled system with the TDE mechanism displayed a shorter rise (RT) when the TDE was introduced. In addition, the TDE mechanism in the TDE-PESO-ADRC showed a decrease in overshoot at the beginning of the transient response, contrary to the slight increase in response obtained in the TDE-PID controller

between 0 and 5 s for the case of added disturbance $f_1(x(t), t)$ given by Equation (21). However, for the TDE-PID controller with added disturbance in Equation (21), the overshoot decreased by 14% between 20 and 25 seconds. For the PESO-ADRC controller, the system response was unstable at the onset of the external disturbance in the absence of TDE. Thus, the response could not be plotted.

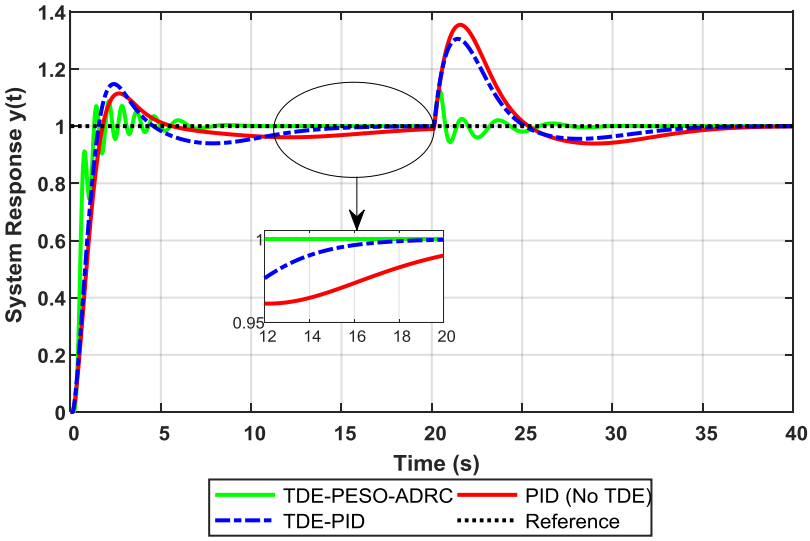

Figure 9. Case 1: System response impact of TDE on PID and PESO-ADRC methods under nonlinear hysteresis, perturbed parameters, and added disturbance $f_1(x(t), t)$.

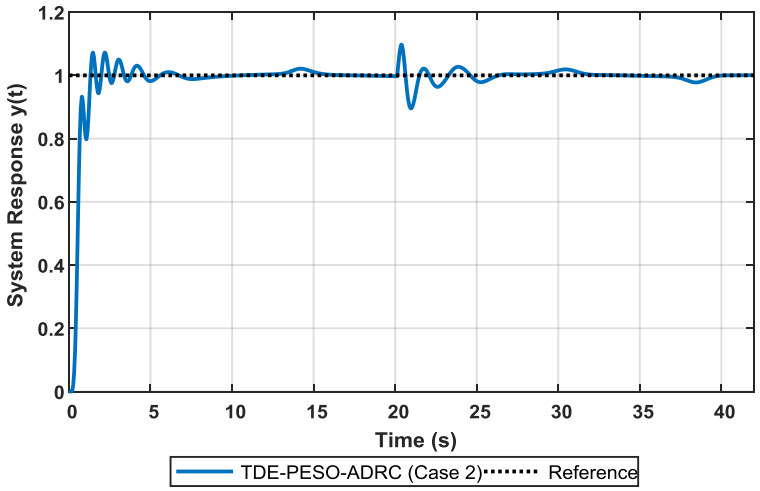

Figure 10. Case 2: System response impact of TDE on PESO-ADRC method under nonlinear hysteresis, perturbed parameters, and added disturbance $f_2(x(t), t)$.

Moreover, employing the TDE mechanism to control the perturbed system under the effect of periodic disturbance $f_2(x(t), t)$ given by Equation (22) is pictorially presented in Figure 10. The system's response characteristics are provided in Table 4. For both cases, with the TDE mechanism, the predictive-based ADRC's response shows system instability after adding an external disturbance to the perturbed time-delay system under nonlinear hysteresis. Thus, the system response for the same is not plotted in both Figures 9 and 10. Therefore, the improvement values [P_i (%)] could not

be tabulated in Table 4 for the PESO-ADRC controller method. However, by incorporating the TDE mechanism in this circumstance, the TDE-PESO-ADRC could conquer this unsteady behavior and provide an acceptable response curve that demonstrated considerable resistance to system uncertainties (Figure 10 and Table 4).

Table 4. Control performance criteria for PID and PESO-ADRC controllers under hysteresis, parameter perturbation, and added external disturbance.

Control method	Performance criteria	TDE excluded	TDE included*	TDE included**	P_i (%)
PID	RT (s)	1.1644	1.0237	Unstable	12.0835
	ST (s)	34.0669	31.9926	Unstable	6.0889
	OV (%)	35.5585	30.5462	Unstable	14.0959
	ITAE	40.4700	30.4100	Unstable	24.8579
PESO-ADRC	RT (s)	Unstable	0.3836	0.3741	-
	ST (s)	Unstable	23.7901	9.6750	-
	OV (%)	Unstable	12.6710	33.4131	-
	ITAE	Unstable	4.3900	7.9730	-

**Case 1, **Case 2*

Similarly, both Figure 10 and Table 4 do not include the system response's performance measures for the TDE-PID method because of the oscillatory character of the periodic external disturbance given in Equation (22) added to the system under test, seen in Equation (18). Hence, it is inferred that the TDE-PESO-ADRC control method is less susceptible to different forms of input disturbances like periodic, nonlinear, and step forms applied to the concerned controlled object, in contrast to the TDE-PID control mechanism. Therefore, this emphasizes how crucial the TDE control mechanism is for analyzing and mitigating all kinds of nonlinear phenomena subjected to a time-delayed system under control.

3.5. Experiment 5: Impact of TDE on control mechanisms in the presence of nonlinear hysteresis, perturbed system parameter, added external disturbance, and varying system time delay

The robustness of the suggested TDE-PESO-ADRC and TDE-PID techniques is evaluated in this experiment over a range of system delay values when hysteresis, parameter perturbation, and input disturbance are added externally to a system. The delay τ_s in this experimental test is equivalent to the concerned system's time delay (in Figures 11 and 12).

For the ADRC, ω_e = 4, and the TDE parameters are η = 0.001 and t_s = 0.001 s. For hysteresis, the variables used are γ = 0.1, α = 1.16, and β = 0.35. For the PID controller, the TDE parameters considered are η = 0.01 and t_s = 0.001 s, and for hysteresis, the variables used are γ = 2, α = 1.16, and β = 0.35. In this analysis, the input disturbance added externally at 15 s to the perturbed system under control is given by $f_1(x(t), t)$ indicated by Equation (21). Further, 25% of parameter perturbation is injected at 20 s for the TDE-PESO-ADRC method (Figure 11). While assessing the resilience of the TDE-based controllers in this analysis, the delay block present in the input channel of the ESO and the ESPO subsystem, seen in Figure 4, has a value of 0.1 s. This delay is referred to as a delay design in this test. On the other hand, τ_s is varied through a range of known delay values in this experiment to evaluate for robustness. Their corresponding performance index

measures are tabulated in Tables 5 and 6, and the system responses to study the impact of varying time delays are presented in Figures 11 and 12.

For the TDE-based PESO-ADRC controller in Figure 11, the experiments were performed on an increase in delay from τ_s = 0.12 and 0.14 to 0.16 s. It is seen that the system responses were therefore oscillatory for greater system latencies, but they could compensate for nonlinear uncertainties, demonstrating decent strength and steady performance for distinct delay scenarios. Besides the transient response features like RT, OV, and ITAE, Table 5 also lists the response time (t_r), which provides the time needed for the system response to reach a steady state after overcoming the external disturbance applied.

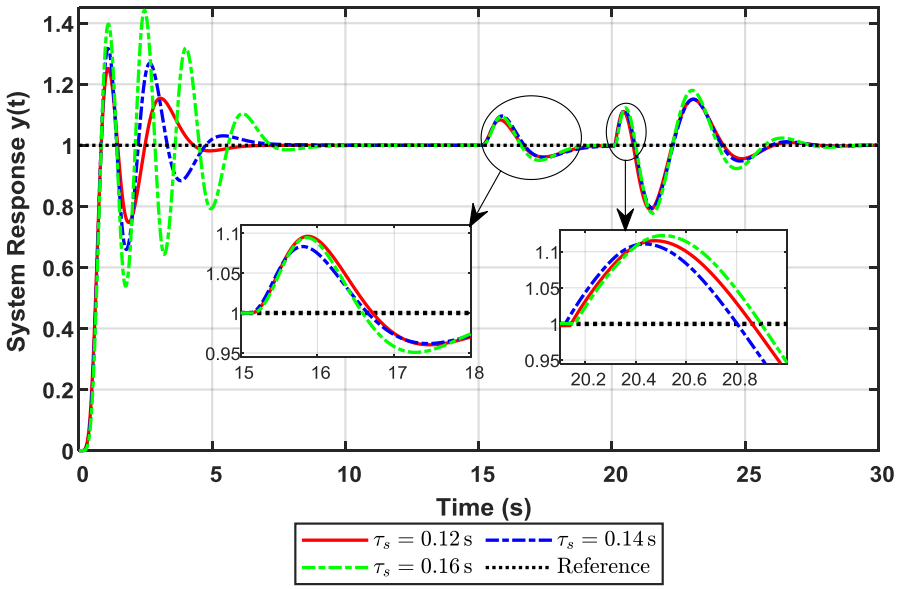

Figure 11. System response for varying system delays for TDE-PESO-ADRC control under nonlinear hysteresis, perturbed parameters, and added disturbance $f_1(x(t), t)$.

Table 5. Comparative analysis of control performance for the TDE-PESO-ADRC approach for change in system delays.

TDE-PESO-ADRC	RT (s)	t_r (s)	OV (%)	ITAE
τ_s = 0.12 s	0.3804	25.5991	25.1663	14.0400
τ_s = 0.14 s	0.3634	25.5840	31.6383	14.9900
τ_s = 0.16 s	0.3512	26.6227	44.0313	18.8000

Further, for the TDE-PID-based controller, the peak values of the oscillating response were decreased for different time-delay situations, such as τ_s = 0.2 s, 0.4 s, and 0.6 s, following the onset of the external disturbance given by Equation (21) and 25% parameter perturbation at 30 s (as seen in Figure 12). Furthermore, the performance criteria displayed in Table 6 for changes in the TDE-PID controlled system delay responses showed robustness and significant compensation for all forms of disturbances present. However, the response curve oscillates for delay values of 0.5 s and above, paving the way for further research. Therefore, it was observed that the TDE-PID controlled system could withstand greater delay values up to 0.6 s, unlike the TDE-PESO-ADRC control method, which could compensate for a second-order system having 0.16 s delay, subjected to various

disturbances and nonlinear backlash-like hysteresis under time-delay control. Thus, this showcases the more robust and endurance behavior of the TDE-PID control method when affected by variations in system time delay.

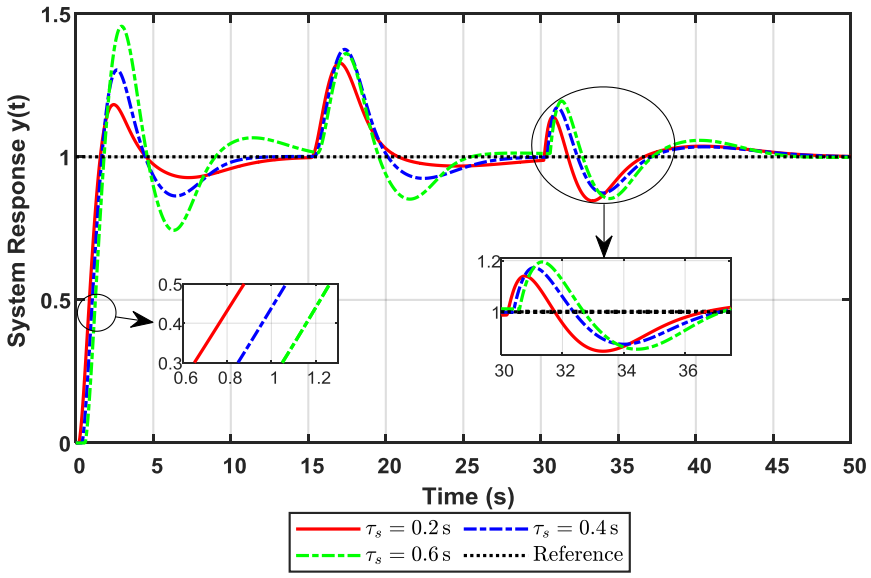

Figure 12. System response for varying system delays for TDE-PID control under nonlinear hysteresis, perturbed parameters, and added disturbance $f_1(x(t), t)$.

Table 6. Comparative analysis of control performance for the TDE-PID control approach for change in system delays.

TDE-PID	RT (s)	t_r (s)	OV (%)	ITAE
τ_s = 0.2 s	0.9958	44.0616	32.6118	54.3800
τ_s = 0.4 s	0.9320	43.9519	37.4193	58.2000
τ_s = 0.6 s	0.8935	44.1372	45.9028	71.7600

3.6. Experiment 6: Control signal for TDE-based controllers

In this section, the parameter values used for the TDE-based controllers are the same as those in the preceding section. The control signals fed to the system under control are provided in Figures 13(a) and 13(b) for TDE-PESO-ADRC and TDE-PID control, respectively. Both responses seen in Figure 13 are under the impact of nonlinear hysteresis, parameter perturbation, and an added external disturbance ($f_1(x(t), t)$), under varying system time-delay scenarios.

For TDE-PESO-ADRC control, the controlled object could withstand smaller delay values (seen in Figure 11 and Table 5). Meanwhile, for TDE-PID control, the controlled object showed resilience to higher system delay values (shown in Figure 12 and Table 6). Hence, the control signals were plotted for each TDE-based control method as per the simulations performed in this section. Figure 13 (a) shows that the TDE-PESO-ADRC method reached a steady state much earlier for a range of smaller, varying time-delay values. However, the TDE-PID control method took longer to achieve a steady state, as seen in Figure 13 (b). It is to be noted that the TDE-PID is more aggressive at the beginning of the control (the control signal reaches 11), which might trigger hard constraints for some applications. Therefore, the controller operations are challenged by adding a hard constraint

on the control signal to the system, with their respective plots shown in Figure 14. This is achieved by inserting a saturation block before the nonlinear hysteresis phenomenon, which leads to the controlled object shown in Figures 4 and 5. In this scenario, the overall system comprises hysteresis, the concerned system with time delay, and other uncertainties acting on it. The saturation block is set to an upper limit of 5 and a lower limit of -5. In Figures 14 and 15, τ_s = 0.12 s for the TDE-PESO-ADRC method, and with τ_s = 0.2 s for the TDE-PID control method.

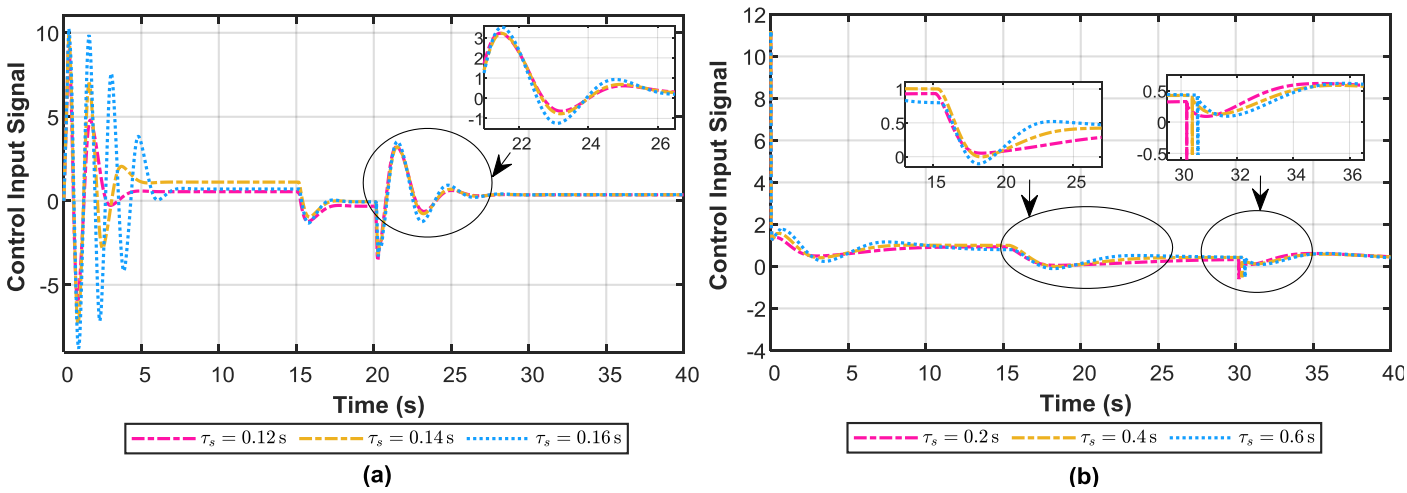

Figure 13. Control signal for varying system delays under nonlinear hysteresis, perturbed parameters, and added disturbance: (a) TDE-PESO-ADRC control; (b) TDE-PID control.

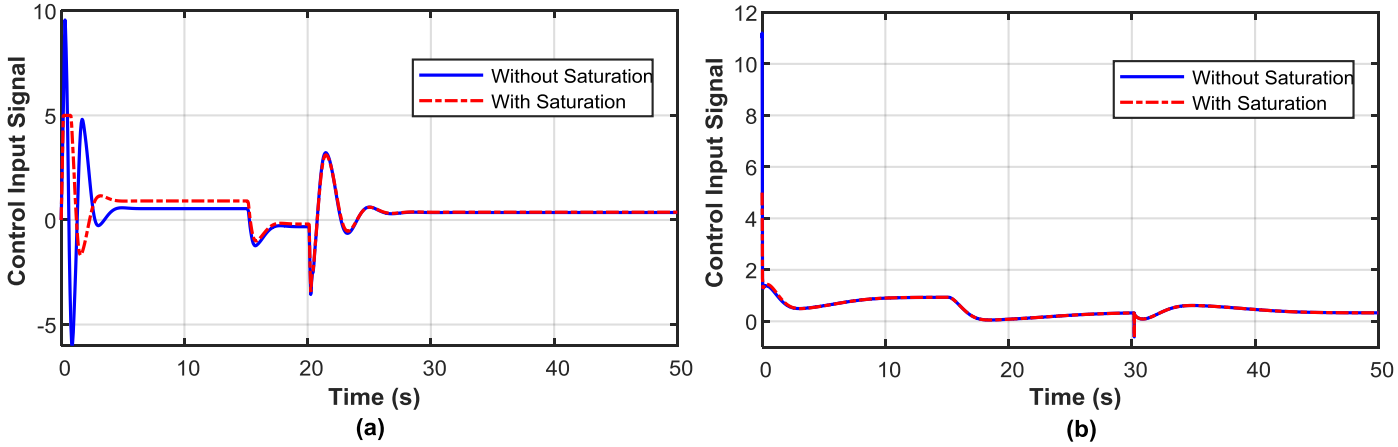

Figure 14. Control signal to the overall system under nonlinear hysteresis, perturbed parameters, and added disturbance for the saturation case: (a) TDE-PESO-ADRC; (b) TDE-PID control.

As observed in Figure 14(a), for the TDE-PESO-ADRC method, the initial amplitude of the control signal is reduced from almost 10 to 5. Moreover, for the TDE-PID control method, the initial peak is reduced from 11 to 5. Therefore, the saturation block further limits the control signal fed to the overall system, making it less aggressive in nature, as seen in Figure 14. Furthermore, Figure 15

provides the corresponding system output responses for the case of saturation added in Figure 14. For both the TDE-PESO-ADRC and TDE-PID control methods, it is noted that the output response curves obtained with saturation present are in accordance with those obtained from the non-saturation case. Hence, an acceptable minimal difference is observed in the output responses by limiting the value of the control signal to the overall system.

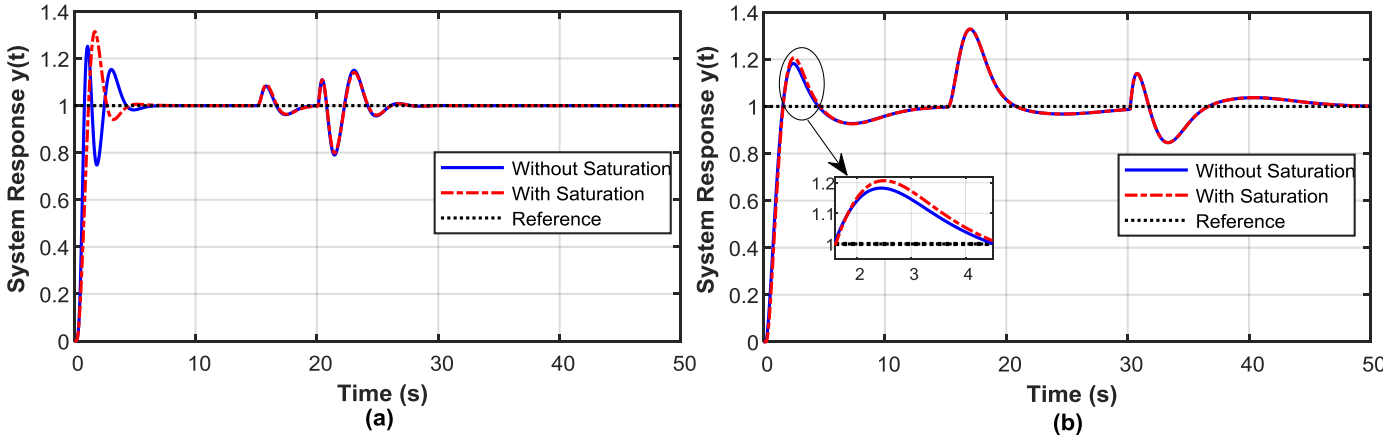

Figure 15. System output response for the saturation case: (a) TDE-PESO-ADRC; (b) TDE-PID control.

3.7. Experiment 7: Sensitivity analysis of the TDE parameters on control mechanisms in the presence of nonlinear hysteresis

This subsection conducts a sensitivity analysis to determine the choice of TDE parameters used for experimentation. Figure 16 illustrates the choice of TDE parameters for the TDE-PID controller operation, by first keeping the positive constant η varying from values 0.001 to 0.2 (in Figure 16 (a)), when b = 0.2. Similarly, in Figure 16 (b), the parameter η is kept fixed at 0.001 for a varying gain factor b value ranging from 0.001 to 0.2.

The significance of parameters η and b are related to the TDE-PID control law $u_t(t)$ given by Equation (16). Figure 16 (a) plots the sensitivity performance for η values tuned to 0.001, 0.01, 0.1, and 0.2, and the gain factor b constant at 0.2. It is noted that the transient response characteristics measured, such as the RT, ST, OV, and ITAE, remain consistent for all the abovementioned η values. Therefore, this indicates that the TDE-PID controlled system is less sensitive to changes in η. Further, Figure 16 (b) illustrates the performance analysis for the case where the parameter b is varied from 0.001, 0.01, 0.1, to 0.2; and for all η = 0.001. Hence, it is seen that the performance criteria measures experience certain changes when b of the TDE-PID controller is varied, but these variations observed are within acceptable limits, hence showcasing less sensitivity to varying b parameter in a relatively small range.

Moreover, a sensitivity performance analysis was conducted on the choice of TDE parameters for the TDE-PESO-ADRC control method. It can be inferred from Figure 17 that for η values tuned to 0.001, 0.01, 0.1, and 0.2, the performance appears to increase slightly for all transient response characteristics (RT, ST, OV, ITAE). Hence, the TDE-PESO-ADRC control method is less sensitive to η values. It is important to note that the parameter b is not included in the control law of TDE-PESO-ADRC, given by Equations (13) and (14); therefore, it has not been plotted in Figure 17.

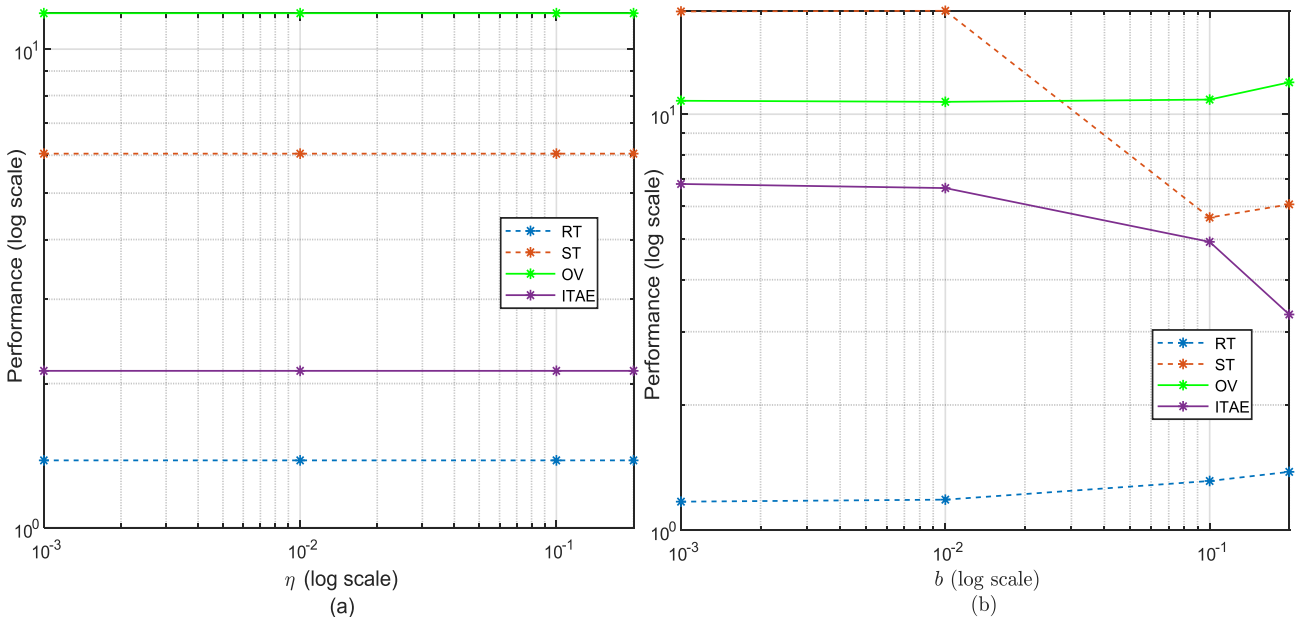

Figure 16. Sensitivity analysis of the TDE-PID control: (a) with constant b parameter; (b) with constant η parameter.

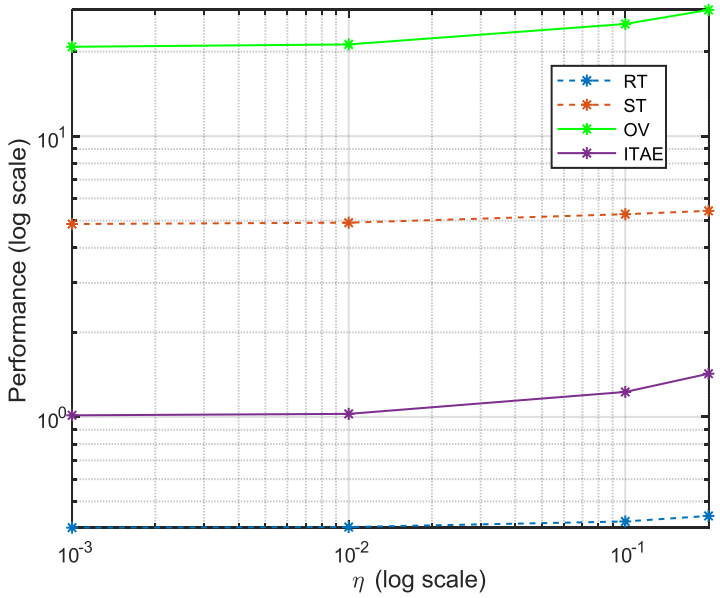

Figure 17. Sensitivity analysis of the TDE-PESO-ADRC control with varying η values.

4. Conclusions

This paper performs a comparative analysis between two recent time-delay estimation-related controllers, namely the TDE-based predictive ESO-based ADRC method [8] and the TDE-based PID control method [17], to highlight the importance of TDE methods in predicting and overcoming the various uncertainties and nonlinearities manifested in the control system theory field.

The experiments performed in this paper were tested using the TDE-based controllers on a

second-order time-delay system under different circumstances, such as the presence of nonlinear backlash-like hysteresis, followed by system parameter perturbation, then an external input disturbance, followed by varying the perturbed system's time delay. Under all these scenarios, the TDE-PESO-ADRC approach improved the estimation and mitigation of the uncertain prevailing nonlinearities compared to its non-TDE counterpart. Also, the TDE-PID controller showed good robustness to various uncertainties, with shorter rise time and settling time, stable system response, and decreased oscillations. The results obtained were validated using measures such as performance index metrics and transient response characteristics. Furthermore, a sensitivity analysis was conducted on the choice of specific TDE parameters for TDE-based controllers to validate their respective selected values.

However, it was demonstrated that the TDE-PESO-ADRC method could estimate and counteract the different forms of periodic and step forms of external disturbances added to the perturbed system to be controlled, unlike the TDE-PID controller, which showed an unstable response under the impact of a periodic kind of disturbance, hence directing the use of adaptive TDE gains under future scope. On the other hand, the TDE-PID control approach could sustain a satisfactory and stable response to an increasing system time delay, unlike the TDE-PESO-ADRC method, which showed endurance to a small range of carrying system time delay. Therefore, future work is required to obtain a decent trade-off by improving the TDE-based control mechanism for systems with unknown and higher delay values, along with considering noise and friction acting on a higher-order system under control. Currently, the setup of a hardware-based human-machine interface platform is underway, followed by the modeling of its digital twin setup. These time-delay estimation-based controllers will be combined with the modeled digital twin to minimize the error signal between the physical system output and the digital twin output. Hence, the control and time-delay compensation of such higher-order systems will contribute to real-world industrial applications.

Author contributions

Syeda Nadiah Fatima Nahri: conceptualization, methodology, software, investigation, validation, formal analysis, writing – original draft preparation, writing – review & editing; Shengzhi Du: conceptualization, methodology, software, validation, writing – review & editing, supervision; Barend J. van Wyk: validation, writing – review & editing; Oluwaseun Kayode Ajayi: writing – review & editing. All authors have read and agreed to the published version of the manuscript.

Use of Generative-AI tools declaration

The authors declare they have not used Artificial Intelligence (AI) tools in the creation of this article.

Acknowledgments

We thank Tshwane University of Technology and the National Research Foundation for granting us the resources and assistance needed for this research study. Moreover, this work is based on the research supported in part by the National Research Foundation of South Africa (grant

numbers PSTD2204143453 and SRUG2203291049).

Conflict of interest

All authors declare no conflicts of interest in this paper.

References

1. Liu Y, Li H, Lu R, Zuo Z, Li X (2022) An overview of finite/fixed-time control and its application in engineering systems. *IEEE/CAA J Automatica Sinica* 9: 2106–2120. https://doi.org/10.1109/JAS.2022.105413
2. Nahri SNF, Du S, Van Wyk BJ (2022) A Review on Haptic Bilateral Teleoperation Systems. *J Intell Robotic Syst* 104: 1–23. https://doi.org/10.1007/s10846-021-01523-x
3. Rahimi F, Mahboobi Esfanjani R (2024) Estimating tolerable communication delays for distributed optimization problems in control of heterogeneous multi-agent systems. *IET Control Theory Appl* 18: 626–639. https://doi.org/10.1049/cth2.12595
4. Chen W-H, Yang J, Guo L, Li S (2015) Disturbance-observer-based control and related methods—An overview. *IEEE T Ind Electron* 63: 1083–1095. https://doi.org/10.1109/TSMC.2023.3240751
5. Nahri SNF, Du S, van Wyk BJ, Denzel Nyasulu T (2024) Mitigating the Time Delay and Parameter Perturbation by a Predictive Extended State Observer-based Active Disturbance Rejection Control. *Annual Conference Towards Autonomous Robotic Systems*, 256–269. https://doi.org/10.1007/978-3-031-72059-8_22
6. Gao Z (2014) On the centrality of disturbance rejection in automatic control. *ISA Trans* 53: 850–857. https://doi.org/10.1016/j.isatra.2013.09.012
7. Han J (2009) From PID to Active Disturbance Rejection Control. *IEEE T Ind Electron* 56: 900–906. https://doi.org/10.1109/TIE.2008.2011621
8. Nahri SNF, Du S, van Wyk BJ, Nyasulu TD (2024) Time-Delay Estimation Improves Active Disturbance Rejection Control for Time-Delay Nonlinear Systems. *Machines* 12: 552. https://doi.org/10.3390/machines12080552
9. Han JQ (1998) Auto Disturbance Rejection Controller and It's Applications. *Control and decision* 13: 19–23.
10. Fareh R, Khadraoui S, Abdallah MY, Baziyad M, Bettayeb M (2021) Active disturbance rejection control for robotic systems: A review. *Mechatronics* 80: 102671. https://doi.org/10.1016/j.mechatronics.2021.102671
11. Sun L, Xue W, Li D, Zhu H, Su ZG (2021) Quantitative tuning of active disturbance rejection controller for FOPTD model with application to power plant control. *IEEE T Ind Electron* 69: 805–815. https://doi.org/10.1109/TIE.2021.3050372
12. Gu S, Zhang J, Liu X (2024) Event-Triggered Finite-Time Variable Gain ADRC for Master–Slave Teleoperated Parallel Manipulators. *IEEE Transactions on Circuits and Systems II: Express Briefs* 71: 3383–3387. https://doi.org/10.1109/TCSII.2024.3359318
13. Li J, Zhang L, Li S, Mao Q, Mao Y (2023) Active disturbance rejection control for piezoelectric smart structures: A review. *Machines* 11: 174. https://doi.org/10.3390/machines11020174

14. Pham TT, Nguyen CN (2023) Adaptive PID sliding mode control based on new Quasi-sliding mode and radial basis function neural network for Omni-directional mobile robot. *AIMS Electronics & Electrical Engineering* 7: 121–134. https://doi.org/10.3934/electreng.2023007
15. Ran M, Wang Q, Dong C, Xie L (2020) Active disturbance rejection control for uncertain time-delay nonlinear systems. *Automatica* 112: 108692. https://doi.org/10.1016/j.automatica.2019.108692
16. Chen S, Xue W, Zhong S, Huang Y (2018) On comparison of modified ADRCs for nonlinear uncertain systems with time delay. *Sci China Inform Sci* 61: 1–15. https://doi.org/10.1007/s11432-017-9403-x
17. Nahri SNF, Du S, Van Wyk B, Ajayi OK, Nyasulu TD, Yu H (2025) Improvement of Proportional-Integral-Derivative Control for Time-Delay Nonlinear Systems by a Time-Delay Estimation Method. *2025 33rd Southern African Universities Power Engineering Conference (SAUPEC 2025)*, 1–6. IEEE. https://doi.org/10.1109/SAUPEC65723.2025.10944363
18. Wang Y, Peng J, Zhu K, Chen B, Wu H (2020) Adaptive PID-fractional-order nonsingular terminal sliding mode control for cable-driven manipulators using time-delay estimation. *Int J Syst Sci* 51: 3118–3133. https://doi.org/10.1080/00207721.2020.1808732.
19. Taefi M, Khosravi MA (2024) A model free adaptive-robust design for control of robot manipulators: time delay estimation approach. *Int J Robust Nonlinear Control* 34: 8227–8247. https://doi.org/10.1002/rnc.7379
20. Glida HE, Chelihi A, Abdou L, Sentouh C, Perozzi G (2023) Trajectory tracking control of a coaxial rotor drone: Time-delay estimation-based optimal model-free fuzzy logic approach. *ISA T* 137: 236–247. https://doi.org/10.1016/j.isatra.2022.12.015
21. Ahmed S, Ghous I, Mumtaz F (2024) TDE based model-free control for rigid robotic manipulators under nonlinear friction. *Scientia Iranica* 31: 137–148. https://doi.org/10.24200/sci.2022.57252.5141
22. Anjum Z, Zhou H, Guo Y (2022) Self-tuning fuzzy nonsingular proportional-integral-derivative type fast terminal sliding mode control for robotic manipulator in the presence of backlash hysteresis. *Transactions of the Institute of Measurement and Control* 44: 809–819. https://doi.org/10.1177/01423312211013330
23. Zhang Y, Fang L, Song T, Zhang M (2023) Model-free adaptive control based on prescribed performance and time delay estimation for robotic manipulators subject to backlash hysteresis. *Proceedings of the Institution of Mechanical Engineers, Part C: Journal of Mechanical Engineering Science* 237: 5674–5691. https://doi.org/10.1177/09544062231160350
24. Li L, Su Y, Kong L, Jiang K, Zhou Y (2022) TDE-based adaptive super-twisting multivariable fast terminal slide mode control for cable-driven manipulators with safety constraint of error. *IEEE Access* 11: 6656–6664. https://doi.org/10.1109/ACCESS.2022.3232555
25. Li J, Zhang L, Li S, Su J (2023) A time delay estimation interpretation of extended state observer-based controller with application to structural vibration suppression. *IEEE T Autom Sci Eng*. https://doi.org/10.1109/TASE.2023.3253504
26. Ahmed S, Wang H, Tian Y (2019) Adaptive high-order terminal sliding mode control based on time delay estimation for the robotic manipulators with backlash hysteresis. *IEEE Transactions on Systems, Man, and Cybernetics: Systems* 51: 1128–1137. https://doi.org/10.1109/TSMC.2019.2895588

27. Ikhouane F (2018) A survey of the hysteretic Duhem model. *Arch Comput Method Eng* 25: 965–1002. https://doi.org/10.1007/s11831-017-9218-3
28. Jing N, Qiang C, Xuemei R (2018) Chapter 16 - Hysteresis Dynamics and Modeling. In: Jing N, Qiang C, Xuemei R, editors. *Adaptive Identification and Control of Uncertain Systems with Non-smooth Dynamics*, 249–256. https://doi.org/10.1016/B978-0-12-813683-6.00021-0
29. Zhao S, Gao Z (2014) Modified active disturbance rejection control for time-delay systems. *ISA T* 53: 882–888. https://doi.org/10.1016/j.isatra.2013.09.013
30. Nahri SNF, Du S, van Wyk BJ (2023) Predictive Extended State Observer-Based Active Disturbance Rejection Control for Systems with Time Delay. *Machines* 11: 144. https://doi.org/10.3390/machines11020144
31. Xue W, Liu P, Chen S, Huang Y (2016) On extended state predictor observer based active disturbance rejection control for uncertain systems with sensor delay. *2016 16th International Conference on Control, Automation and Systems (ICCAS)*, 1267–1271. IEEE. https://doi.org/10.1109/ICCAS.2016.7832475
32. Borase RP, Maghade D, Sondkar S, Pawar S (2021) A review of PID control, tuning methods and applications. *International Journal of Dynamics and Control* 9: 818–827. https://doi.org/10.1007/s40435-020-00665-4
33. Wen-bin Y, Dong Y (2015) Modeling and Simulation of an Active Disturbance Rejection Controller Based on Matlab/Simulink. *International Journal of Research in Engineering and Science (IJRES)* 3: 62–69.

AIMS Press